Chapter 6

Examination of Rising R-curve Behavior in Bone Using Fiber Bridging Models

6.1 Introduction

Bone is a composite material with a complex hierarchical structure which is imbued with several mechanisms to resist fracture at multiple scales. These scales relate to the characteristic structural dimensions in bone, which vary from tropocollagen at the nanoscale, mineralized collagen fibrils at the scale of tens of nanometers, collagen bundles to form the lamellar structure above micrometer dimensions, to the osteon structures, which are several micrometers in size [1]. It is the simultaneous operation of toughening mechanisms at these different size scales that provides bone with its prominent strength and toughness. The following toughening mechanisms have been reported for cortical bone, including sacrificial bonds between fibrils [2], plasticity ahead of the crack [3], constrained microcrack [4], crack deflection [5, 6] and crack bridging [5]. For individual microcracks, bridging by collagen fibrils might be significant since the substantially smaller collagen fibrils would be able to bridge a large percentage of the crack length.

Crack bridging is one of the so called extrinsic toughening mechanisms which act to shield the crack from part of the applied driving force and operate behind the crack tip in the crack wake. For the materials with extrinsic toughening mechanisms, the fracture

resistance increases with crack extension and stable crack growth can occur before unstable fracture. Rising R-curve behavior is the direct result of extrinsic toughening mechanisms, which cause the crack-size dependence of the toughness. In this chapter, crack bridging by collagen fibrils in toughening cortical bone was first time investigated systematically.

6.2 Fiber Bridging Model

Fiber bridging mechanism can enhance the fracture toughness of the material by providing the bridging-stress across the crack, which reduces the chance that the crack will grow larger.

Let us consider a single crack of $2a$ length bridged by unidirectional fibers under remote tensile stress σ_0 as shown in **Figure 6-1**. A mode I stress intensity is created at the crack tips, which is characterized by the stress intensity factor K_I. According to the linear elastic fracture mechanics, if K_I is greater than the fracture toughness, K_{IC}, of the material, the crack may start propagating leading to the fracture of the material, which is

$$K_I \geq K_{IC} \tag{6.1}$$

If there were no fibers bridging the crack, the stress intensity factor of a Griffith crack of length $2a$ is given by [7]

$$K_{app} = 2\sqrt{\frac{a}{\pi}}\int_0^a \frac{\sigma_0}{\sqrt{a^2 - x^2}}dx \tag{6.2}$$

However, due to the presence of fibers, the crack opening is constrained by the fiber bridging mechanism. The bridging fibers exert a stress $p(x)$ on the crack surfaces which leads to the actual stress intensity factor of the model is

$$K_{tip} = 2\sqrt{\frac{a}{\pi}}\int_0^a \frac{\left[\sigma_0 - p(x)\right]}{\sqrt{a^2 - x^2}}dx = K_{app} - K_{br} \tag{6.3}$$

Since the total stress is shared between the fibers and the matrix, based on the volume-ensemble averaging scheme, we have

$$\sigma_0 = \phi_f \sigma_f^\infty + \left(1 - \phi_f\right)\sigma_m^\infty \tag{6.4}$$

where ϕ_f is the volume fraction of the fiber; σ_f^∞ and σ_m^∞ represent the average axial stresses in the fiber and matrix far away from the crack, respectively. The compatibility condition of the axial strain of the fiber, matrix, and composite leads to the following equation,

$$\frac{\sigma_f^\infty}{E_f} = \frac{\sigma_m^\infty}{E_m} = \frac{\sigma_0}{E^*} \tag{6.5}$$

where E_f and E_m are the Young's moduli of the fiber and matrix, respectively, while E^* denotes the effective Young's modulus of the composite in the fiber direction.

Using the micromechanical framework developed by Ju and Chen [8, 9], E^* can be obtained based on the following effective stiffness tensor of the composite,

$$\boldsymbol{C}^* = \boldsymbol{C}_0 \bullet \left[\boldsymbol{I} + \phi_f\left(\boldsymbol{A} + (1 - \phi_f)\boldsymbol{S}\right)^{-1}\right] \tag{6.6}$$

where

$$\boldsymbol{A} = \left(\boldsymbol{C}_1 - \boldsymbol{C}_0\right)^{-1} \bullet \boldsymbol{C}_0 \tag{6.7}$$

In Eq. (6.6), $\boldsymbol{C}_0$ and $\boldsymbol{C}_1$ represent the stiffness tensor of the matrix and fiber, respectively; $\boldsymbol{S}$ denotes the interior-point Eshelby's tensor for spheroid (cf. **Appendix I**).

Combining (6.4) and (6.5), the axial stress in the fiber far away from the crack can be expressed as

$$\sigma_f^{\infty} = \frac{E_f}{\left(1-\phi_f\right)\left(1+\eta\right)E_m}\sigma_0 \tag{6.8}$$

where

$$\eta = \frac{\phi_f E_f}{\left(1-\phi_f\right)E_m} \tag{6.9}$$

Following Qu and Cherkaoui [10], the stress exerted on the crack surface by the bridging fibers and the crack opening displacement can be derived as followed. As shown in **Figure 6-2**, the center of the fiber is x distance away from the center of the crack. Due to the geometric singularity, the stress fields near the crack surface are quite high, and certain portions of the fiber-matrix interface have failed. Assuming the shear stress on the interface due to friction denoted by τ is a constant, within the debonding of sliding zone, the axial stress in the fiber can be written as

$$\sigma_f\left(z\right) = \sigma_f^{\infty} + \frac{2\tau}{b}z \tag{6.10}$$

where b is the fiber radius. On the basis of Hook's Law, the axial strain in the fiber is

$$\varepsilon_f\left(z\right) = \frac{\sigma_f^{\infty}}{E_f} + \frac{2\tau}{bE_f}z \tag{6.11}$$

The integration of Eq. (6.11) with respect to z leads to the total extension of the fiber within the sliding zone:

$$2\Delta_f(x) = 2\int_0^{l(x)} \varepsilon_f(z)\,dz = 2\left(\frac{\sigma_f^\infty}{E_f} + \frac{\tau l(x)}{bE_f}\right) l(x) \tag{6.12}$$

Similar to Eq. (6.10) and (6.11), by assuming the stress in the matrix within the sliding zone is also a linear function of z, we can write

$$\sigma_m(z) = \left[1 - \frac{z}{l(x)}\right]\sigma_m^\infty \tag{6.13}$$

$$\varepsilon_m(z) = \left[1 - \frac{z}{l(x)}\right]\frac{\sigma_m^\infty}{E_m} \tag{6.14}$$

The integration of Eq. (6.14) gives the axial elongation of the matrix within the sliding zone:

$$2\Delta_m(x) = 2\int_0^{l(x)} \varepsilon_m(z)\,dz = \frac{\sigma_m^\infty}{E_m} l(x) \tag{6.15}$$

The difference between Eq. (6.12) and (6.15) yields the crack opening displacement, $v(x)$:

$$2v(x) = 2\Delta_f(x) - 2\Delta_m(x) = 2\left(\frac{\sigma_f^\infty}{E_f} + \frac{\tau l(x)}{bE_f}\right) l(x) - \frac{\sigma_m^\infty}{E_m} l(x) \tag{6.16}$$

Substituting Eq.(6.5) and (6.8) into Eq.(6.16), we have

$$v(x) = \left[\frac{\tau l(x)}{bE_f} + \frac{\sigma_0}{2\left[\phi_f E_f + (1-\phi_f) E_m\right]}\right] l(x) \tag{6.17}$$

By solving the above equation, one can find

$$l(x) = \frac{\eta\sigma_0 b}{4(1+\eta)\phi_f\tau}\left[\sqrt{1 + \frac{16(1+\eta)^2 E_f \phi_f^2 \tau v(x)}{\eta^2\sigma_0^2 b}} - 1\right] \tag{6.18}$$

In practice, the fiber-bridging stress is finite based on the fiber strength. Furthermore, because of the variability of the fiber strength, it may be reasonable to characterize the probabilistic nature of it by introducing the following equation:

$$\hat{\phi}(x) = \phi_f \left[1 - P_f(x)\right] \tag{6.19}$$

where

$$P_f\left(\phi_f, x\right) = 1 - \exp\left[-\frac{p_1(x)}{\phi_f \sigma_{cr}}\right]^m \tag{6.20}$$

In Eq.(6.19) and (6.20), $\hat{\phi}$ represents the effective volume fraction of the fiber on the crack surface, P_f is the failure probability of the fiber based on Weibull distribution [11], m is the Weibull parameter, and σ_{cr} is the average failure stress of the fiber. It is noted that, in order to predict the extent of the damage, the bridging stress $p_1(x)$ without fiber breakage is considered. Substituing Eq. (6.19) and (6.18) back to Eq.(6.10), the bridging stress exerted on the crack surface can be written as

$$p(x) = \hat{\phi}\sigma_f(l) = \frac{\hat{\phi}}{\phi_f}\frac{\eta\sigma_0}{2(1+\eta)}\left[\sqrt{1 + \frac{16(1+\eta)^2 E_f \phi_f^2 \tau v(x)}{\eta^2 \sigma_0^2 b}} + 1\right] \tag{6.21}$$

Finally, the crack opening displacement is given by [10]

$$\begin{aligned} v(x) &= \frac{2D}{\pi}\int_0^a \left[\sigma_0 - p(t)\right]\log\left|\frac{\sqrt{a^2 - x^2} + \sqrt{a^2 - t^2}}{\sqrt{a^2 - x^2} - \sqrt{a^2 - t^2}}\right| dt \\ &= 2D\sigma_0\sqrt{a^2 - x^2} - \frac{2D}{\pi}\int_0^a p(t)\log\left|\frac{\sqrt{a^2 - x^2} + \sqrt{a^2 - t^2}}{\sqrt{a^2 - x^2} - \sqrt{a^2 - t^2}}\right| dt \end{aligned} \tag{6.22}$$

where

$$D = \sqrt{\left(\frac{A_{11}A_{22}}{2}\right)\left(\frac{2A_{12}+A_{66}}{2A_{11}} + \sqrt{\frac{A_{22}}{A_{11}}}\right)} \tag{6.23}$$

$$A_{11} = \frac{1-\nu^2}{E_2},\ A_{22} = \frac{E_1 - \nu^2 E_2}{E_1^2},\ A_{12} = -\frac{\nu_{23}(1+\nu)}{E_1},\ A_{66} = \frac{1}{G_{12}} \tag{6.24}$$

In Eq. (6.24), it has been assumed that $\nu_f = \nu_m = \nu$. In order to find $v(x)$, a numerical method needs to be employed. Once $v(x)$ is obtained, the fiber-bridging stress $p(x)$ and the stress intensity factor can be easily found from Eq.(6.21) and (6.3).

6.3 Numerical Simulations and Discussions

On the foundation of proposed crack bridging model, a series of numerical simulations are performed to investigate the fracture behaviors of bone at the lamellar level. The parameters used in the model are listed in **Table 6-1**. **Figure 6-3** and **Figure 6-5** illustrate the relations between the fiber-bridging stresses and the far-field stresses. When fiber breakage is not considered, the fiber-bridging stresses increase proportionally to the far-field stresses. However, in the presence of fiber breakage, a higher applied far-field stress doesn't necessarily give rise to a higher fiber-bridging stress; instead, it may trigger a larger amount of fiber breakage, and therefore lowers the fiber-bridging stress. In addition, the fiber-bridging stresses, with the exception of those near the crack tip, are nearly uniformly distributed. In the presence of extensive fiber breakage, the fiber-bridging stresses exist only near the crack tip.

Figure 6-4 and **Figure 6-6** demonstrate the effect of far-field stress on the crack mouth opening displacement. Clearly, the crack mouth opening displacements are

magnified substantially due to the presence of fiber breakage. **Figure 6-7** to **Figure 6-10** show the effect of far-field stress on the stress intensity factor and the bridging stress intensity factor associated with the shear stress on the interface. It is observed, for the bridging stress intensity factor, that there is an asymptotic value as the shear stress on the interface increases to more than 20 MPa, which may support the hypothesis that the interface strength is dominated by electrostatic interactions in biological materials at this scale [3]. **Figure 6-11** and **Figure 6-12** exhibit the effect of the far-field stress and fiber breakage on the stress intensity factor and the bridging stress intensity factor. It is shown that fiber breakage has a prominent effect on both stress intensity factors. As the far-field stress increases, the differences in both stress intensity factors can be easily observed.

The evolutions of the stress intensity factor and the bridging stress intensity factor caused by the crack length and the far-field stress are illustrated with **Figure 6-13** to **Figure 6-16** . As expected, without fiber breakage, the stress intensity factor is always reduced and the bridging stress intensity factor is always increased with the extension of the crack length, which suggests that the crack propagation can be ceased with a certain crack length. A higher applied far-field stress also leads to a higher fiber-bridging stress intensity factor. On the other hand, in the presence of fiber breakage, a higher applied far-field stress triggers a larger amount of fiber breakage resulting in a much smaller bridging stress intensity factor and a higher stress intensity factor. It is shown clearly in **Figure 6-16** that the bridging stress intensity factors are close when the applied far-field stresses are equal to 25 and 100 MPa in our case.

An increase in the bridging stress intensity factor, K_{br}, can be explained by the R or resistance curve concept. According to ASTM E-561, an R-curve is a plot of the crack extension force (i.e. fracture toughness) versus the crack extension, for slow-stable crack propagation, and it describes the toughness development in a material. The qualitative results reflected clearly in **Figure 6-16** showing the bridging stress intensity factor as a function of crack length. In addition, a comparison between rising R-curve behaviors (depicted in **Figure 6-14** and **Figure 6-16**) and bridging stress distributions (**Figure 6-3** and **Figure 6-5**) clearly show a direct correspondence existing between the bridging stress exerted on the crack surfaces and the rising R-curve effect, that is, the higher the magnitude of the bridging stress, the steeper the rise. In other words, the larger the magnitude of the microscopic bridging-stress distributions, the more fracture resistant the material.

In the current literature, there is no experimental data. Nalla et al. [5] used the uniform-traction Dugdale-zone model to estimate the toughness associated with collagen fibrils bridging assuming that the bridging stress on the fibers is 100 MPa, effective area-fraction of the collagen fibers is 0.15, and the bridging-zone length is 10 μm. Their estimation is ~0.08 MPa$\sqrt{m}$ and is on the same order of our results. **Figure 6-17** and **Figure 6-18** depict sliding zone representing the length of fiber that takes part in creating the bridging stress. The estimated values of sliding zone with fiber breakage at the midpoint of microcrack of crack length 50 μm are between 0.77 and 3.7 μm for remote stresses considered. They are reasonable and consistent with the results of Yeni's model

[12] in which the estimated lengths are between 0.55 and 7.7 for all bone-types considered.

In the present study, by taking advantage of cumulative probability density function, crack bridging by collagen fibrils in toughening cortical bone is systematically investigated. It should be noted that the evolution of fiber breakage is loading history dependent in reality; accordingly a more adequate damage evolution law needs to be employed to characterize the history-dependent damage evolution behavior. Moreover, associated with fiber breakage, the crack propagation analysis needs to be carried out to quantify the extent of fracture resistance of cortical bone in the future study.

6.4 Conclusions

On the basis of constant-shear model, the fracture behaviors of human cortical bone at the lamella level are studied with the framework of linear-elastic fracture mechanics combined with multi-scale effective elastic micromechanical model for lamella. The effect of collagen fiber breakage is considered by taking advantage of cumulative probability function or Weibull distribution. The distribution and evolution of fiber bridging stress, crack mouth opening, and stress intensity factor then are analyzed by considering the probable fiber breakage.

Table 6-1. Set of input parameters for the model.

Parameters	Values	Reference
Collagen elastic modulus	2.9 GPa	Sasaki and Odajima [13]
Collagen Poisson's ratio	0.3	-
Apatite crystal bulk modulus	80 GPa	Gilmore and Katz [14]
Apatite crystal shear modulus	45 GPa	Gilmore and Katz [14]
Mineral crystal aspect ratio in fibril	40/3	Akkus [15]
Ultrastructural water and void aspect ratio	1	-
Fibril volume fraction in ultrastructure	0.53	Fritsch and Hellmich [16, 17]
Apatite crystal volume fraction in ultrastructure	0.40	Fritsch and Hellmich [16, 17]
Apatite crystal distribution parameter	0.75	Lees et al. [18] Sasaki et al. [19]
Crack length $2a$	16-160 μm	Yeni et al. [12]
Fibril diameter	0.03-0.2 μm	Weiner et al. [20] Barber [21]
Failure strength of the fibril	120 MPa	Barber [21]

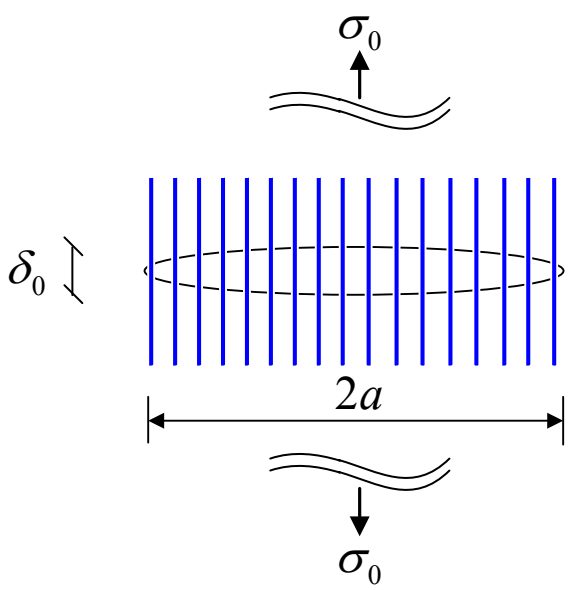

Figure 6-1. A crack of $2a$ length, subjected to the remote stress σ_0 is bridged by unidirectional fibers. δ_0 represents the maximum crack opening displacement.

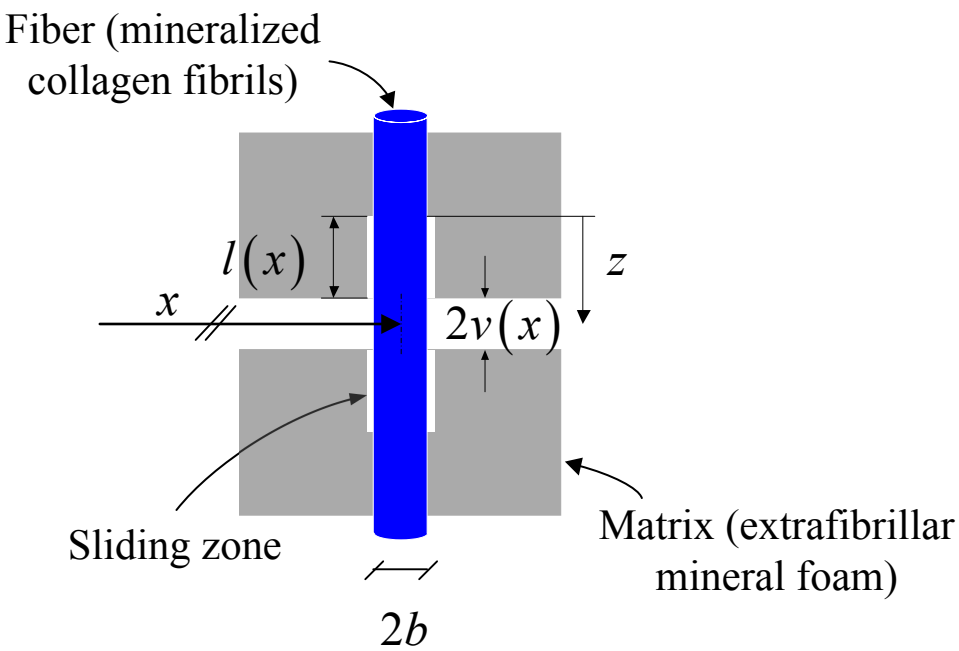

Figure 6-2. Representative element near the crack faces containing a fiber**.**

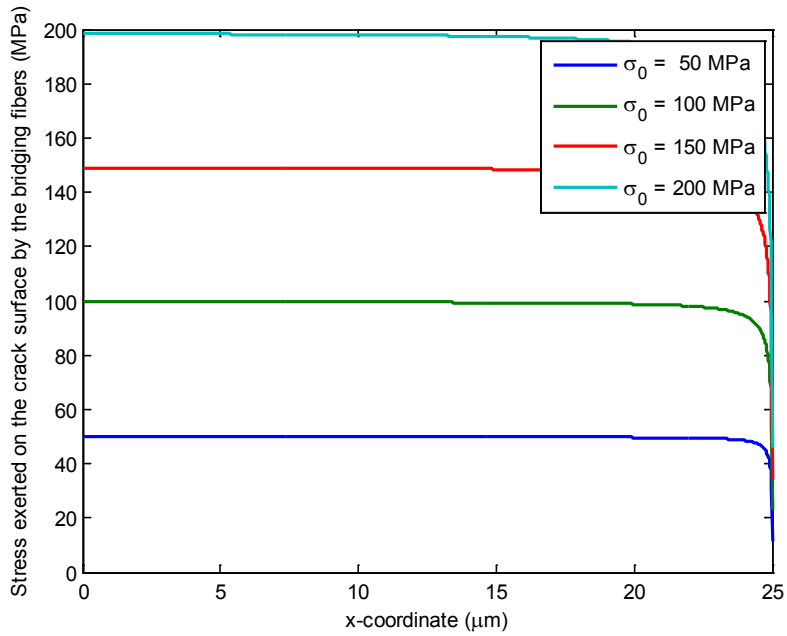

Figure 6-3. The effect of far-field stress on the bridging stress without fiber breakage.

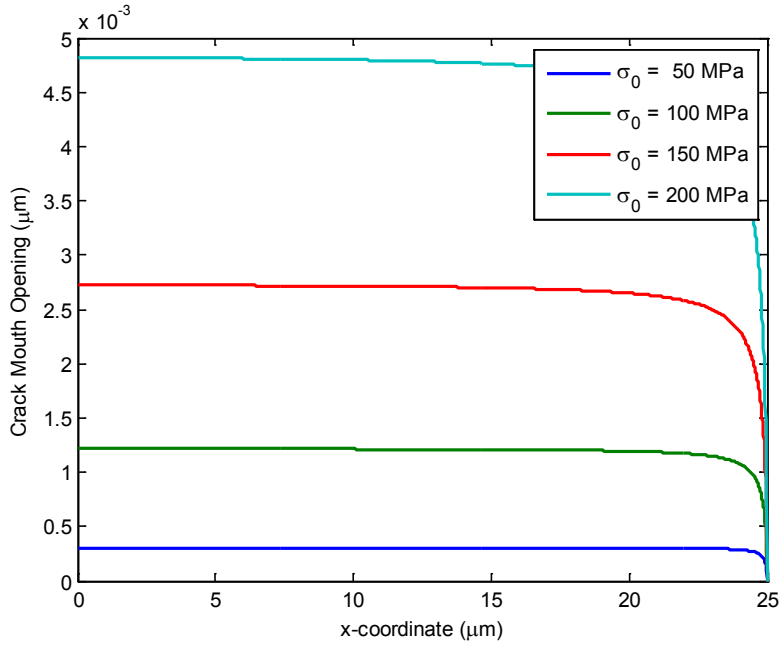

Figure 6-4. The effect of far-field stress on the crack mouth opening displacement without fiber breakage.

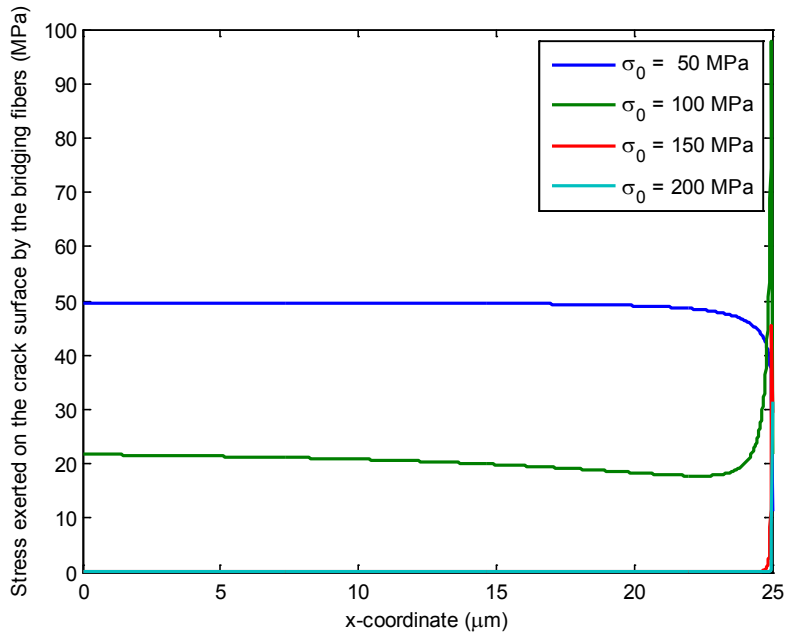

Figure 6-5. The effect of far-field stress on the bridging stress with fiber breakage ($m = 3$, $\tau = 20$ MPa).

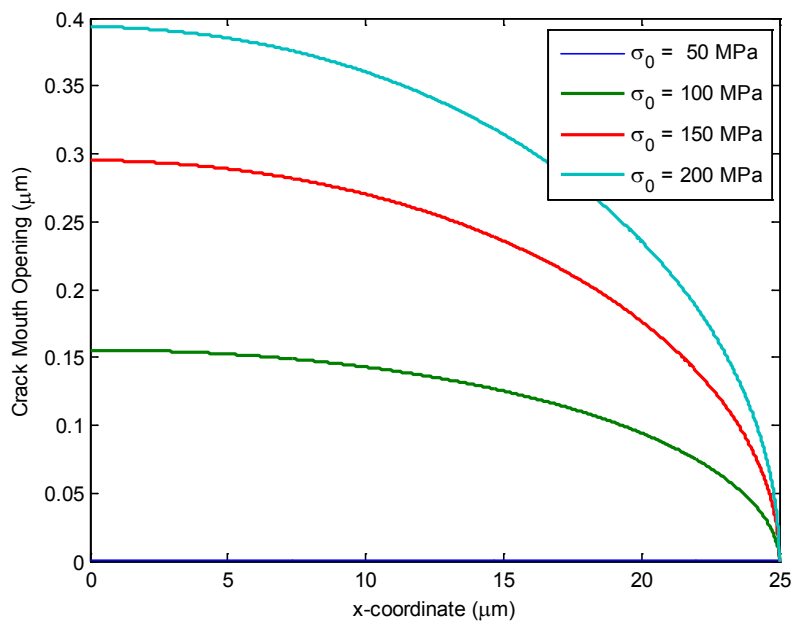

Figure 6-6. The effect of far-field stress on the crack mouth opening displacement with fiber breakage ($m = 3$, $\tau = 20$ MPa).

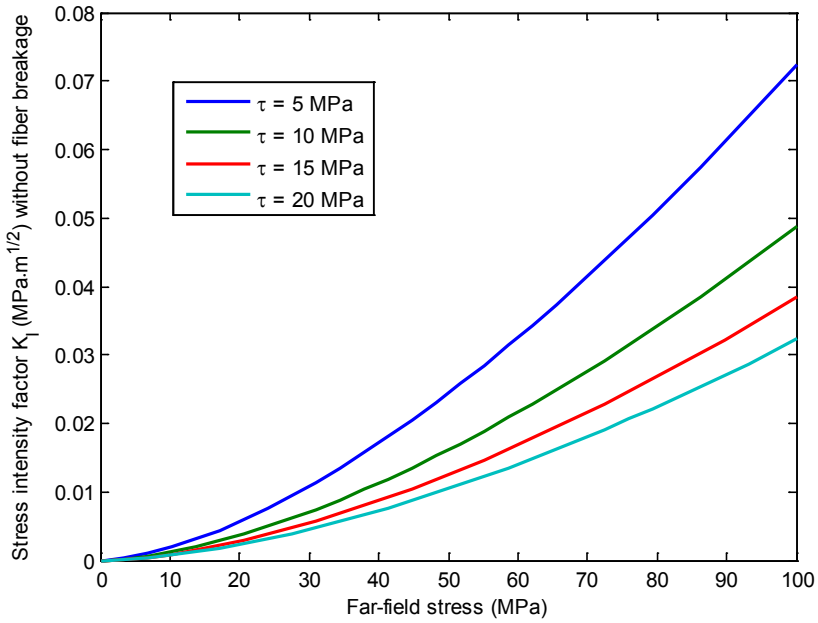

Figure 6-7. The effect of far-field stress on the stress intensity factor without fiber breakage associated with the shear stress.

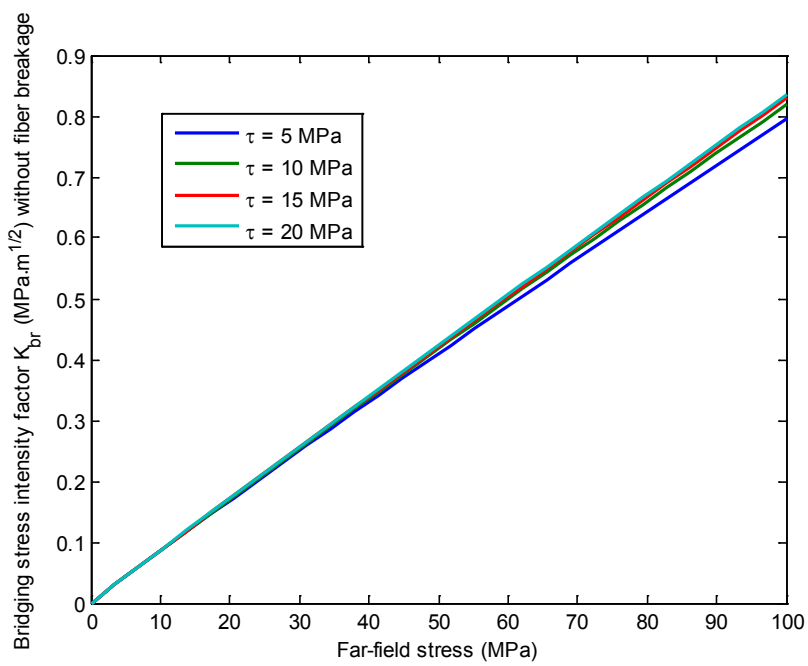

Figure 6-8. The effect of far-field stress on the bridging stress intensity factor without fiber breakage associated with the shear stress.

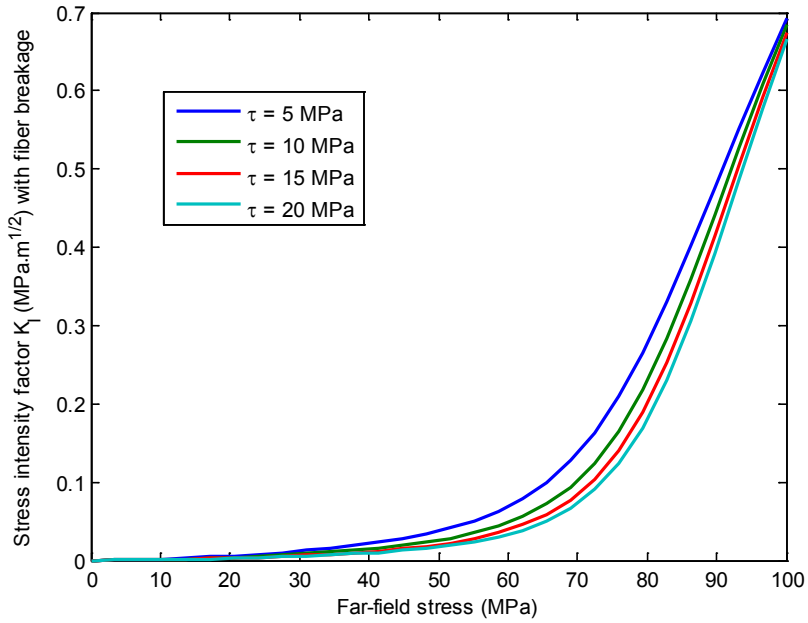

Figure 6-9. The effect of far-field stress on the stress intensity factor with fiber breakage associated with the shear stress (m = 3).

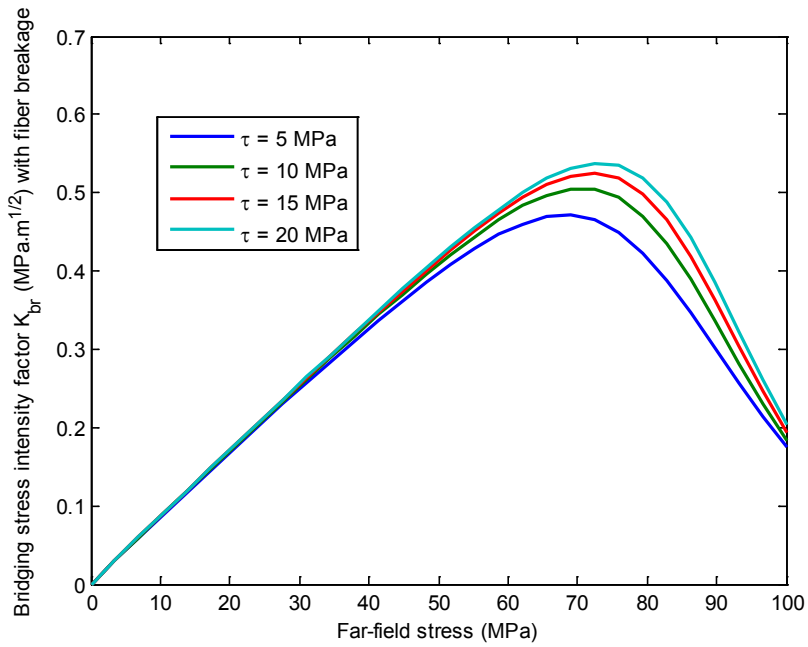

Figure 6-10. The effect of far-field stress on the bridging stress intensity factor with fiber breakage associated with the shear stress (m = 3).

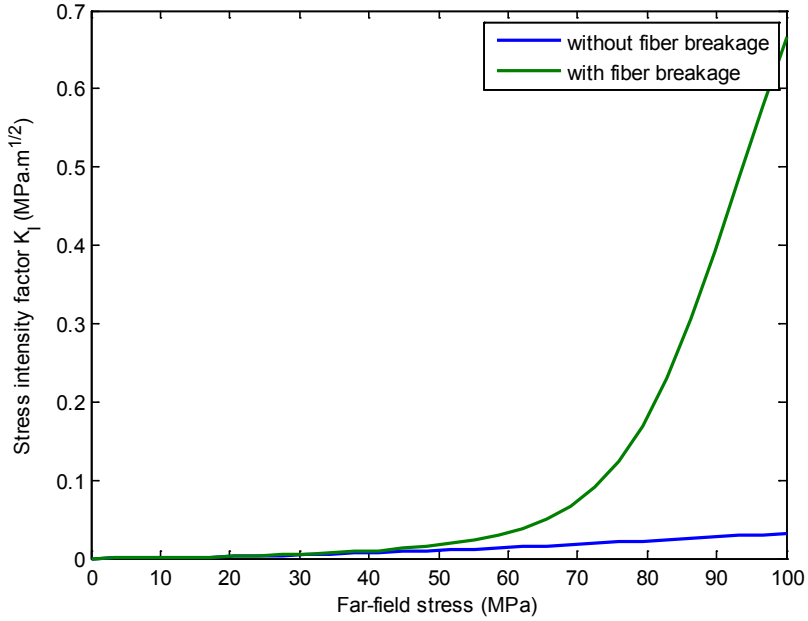

Figure 6-11. The effect of far-field stress on the stress intensity factor (m = 3, τ = 20 MPa).

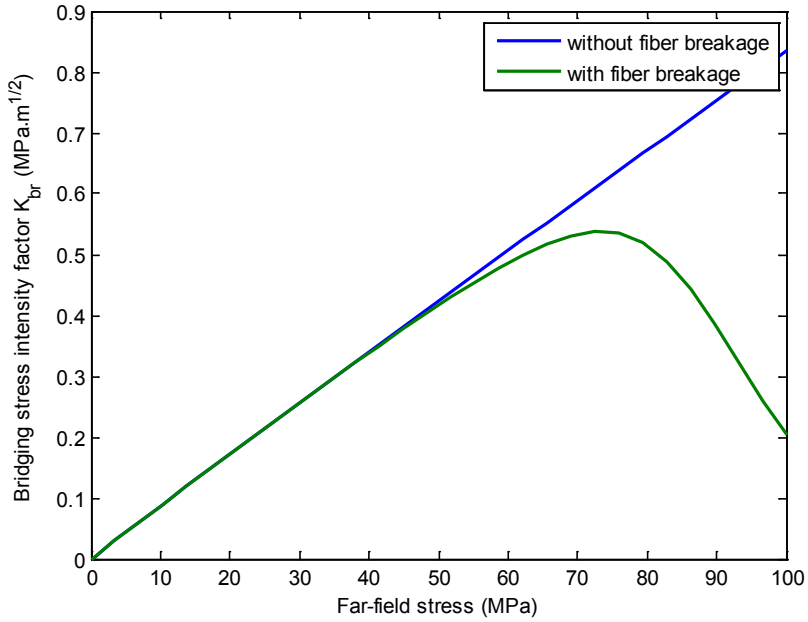

Figure 6-12. The effect of far-field stress on the bridging stress intensity factor (m = 3, τ = 20 MPa).

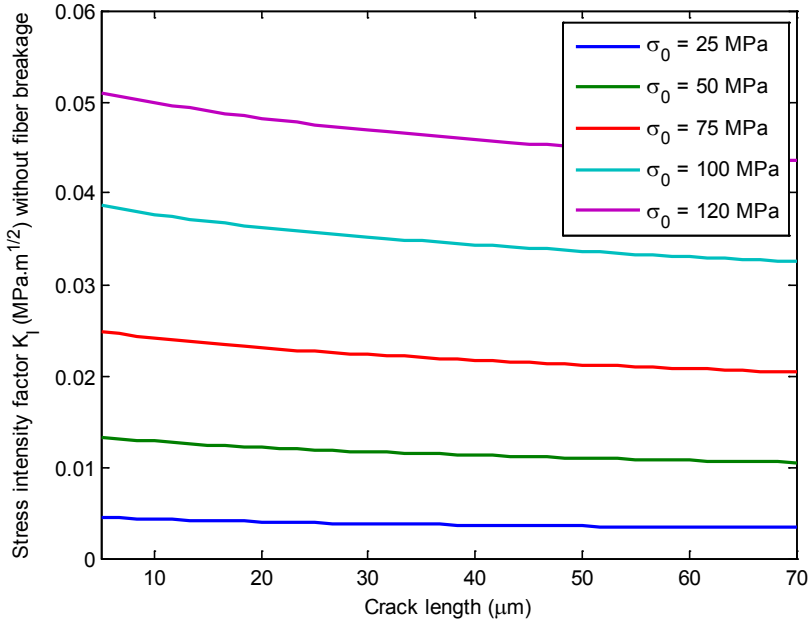

Figure 6-13. The effect of crack length on the stress intensity factor without fiber breakage associated with the far-field stress (m = 3, τ = 20 MPa).

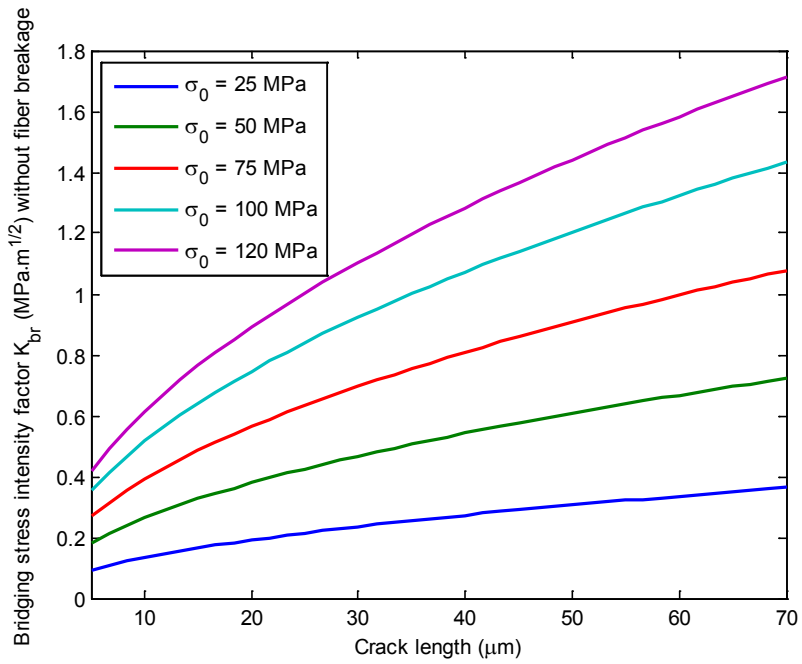

Figure 6-14. The effect of crack length on the bridging stress intensity factor without fiber breakage associated with the far-field stress (m = 3, τ = 20 MPa).

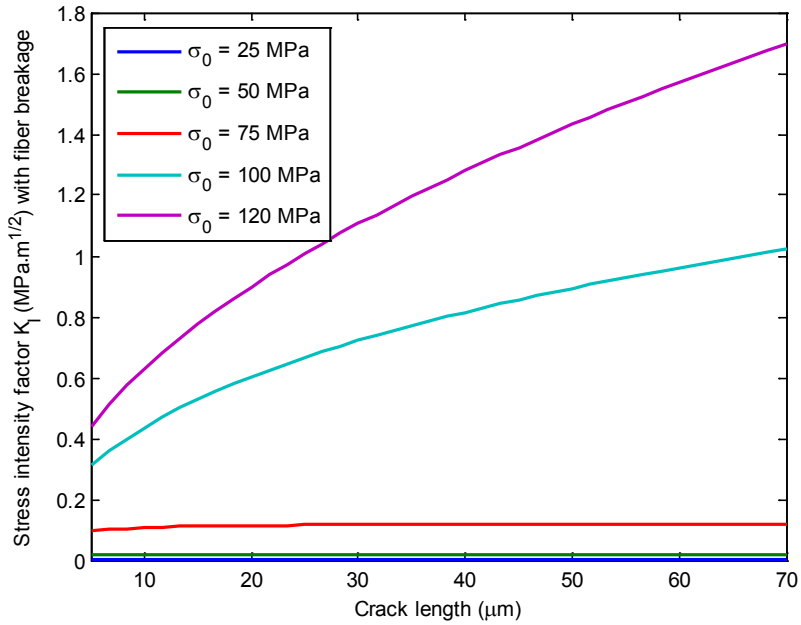

Figure 6-15. The effect of crack length on the stress intensity factor with fiber breakage associated with the far-field stress (m = 3, τ = 20 MPa).

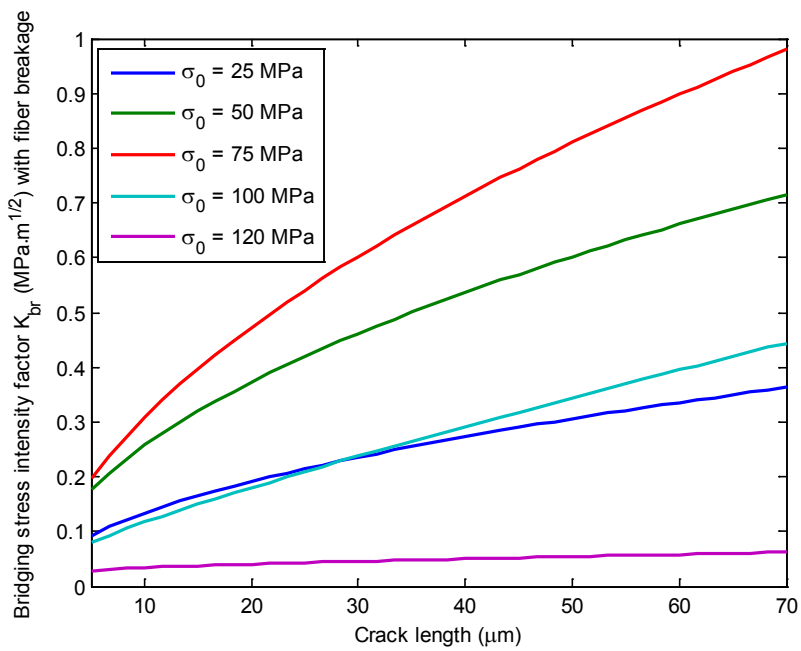

Figure 6-16. The effect of crack length on the bridging stress intensity factor with fiber breakage associated with the far-field stress (m = 3, τ = 20 MPa).

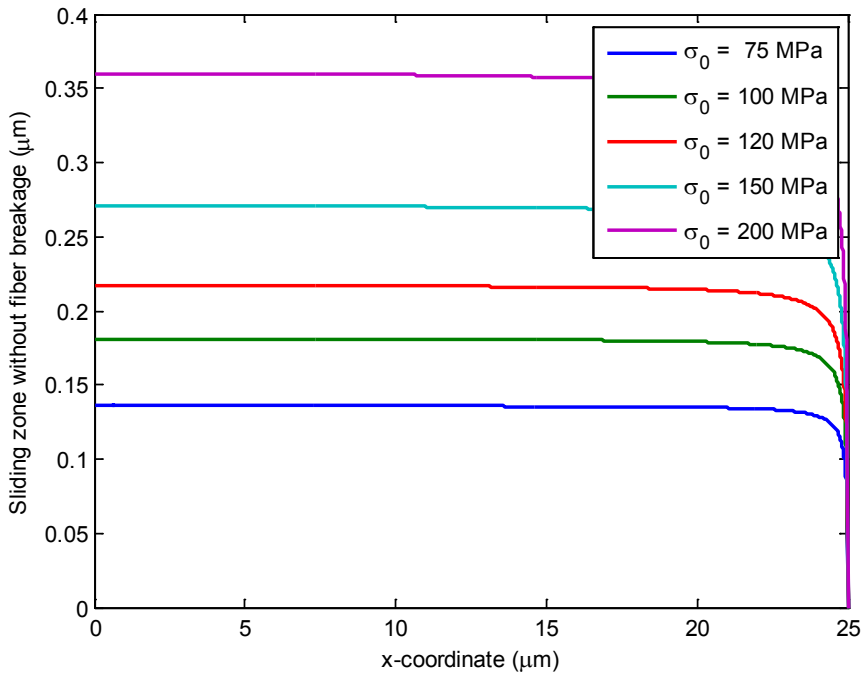

Figure 6-17. Sliding zone without fiber breakage (m = 3, τ = 20 MPa).

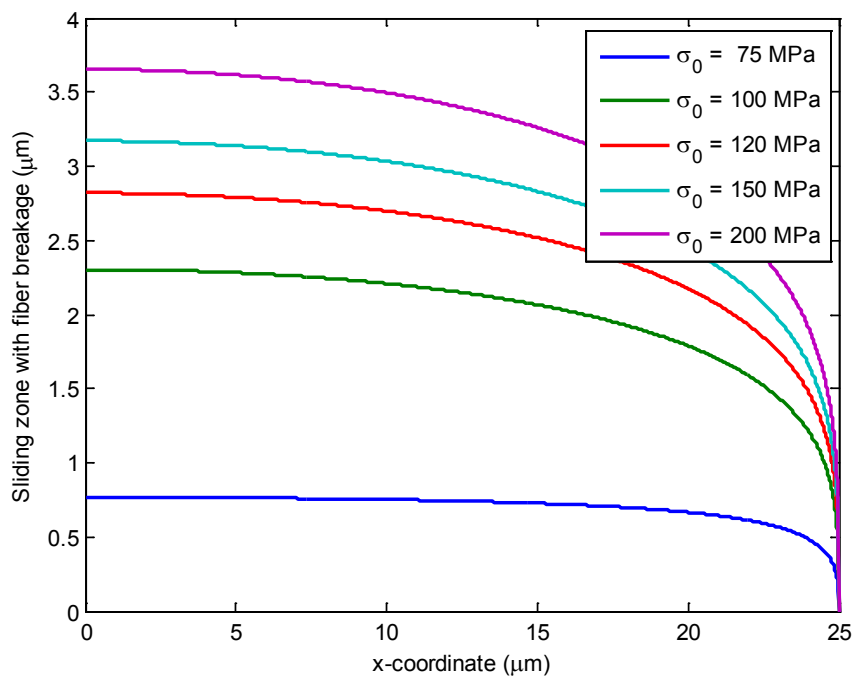

Figure 6-18. Sliding zone with fiber breakage (m = 3, τ = 20 MPa).

6.5 References

1. Launey, M.E., M.J. Buehler, and R.O. Ritchie, *On the Mechanistic Origins of Toughness in Bone.* Annual Review of Materials Research, 2010. **40**(1): p. 25-53.
2. Fantner, G.E., et al., *Sacrificial bonds and hidden length dissipate energy as mineralized fibrils separate during bone fracture.* Nat Mater, 2005. **4**(8): p. 612-616.
3. Baohua, J. and G. Huajian, *Mechanical properties of nanostructure of biological materials.* Journal of the Mechanics and Physics of Solids, 2004. **52**(9): p. 1963-1990.
4. Vashishth, D., K.E. Tanner, and W. Bonfield, *Experimental validation of a microcracking-based toughening mechanism for cortical bone.* Journal of Biomechanics, 2003. **36**(1): p. 121-124.
5. Nalla, R.K., et al., *Fracture in human cortical bone: Local fracture criteria and toughening mechanisms.* J. Biomech., 2005. **38**: p. 1517-1525.
6. Peterlik, H., et al., *From brittle to ductile fracture of bone.* Nature Materials, 2006. **5**(1): p. 52-55.
7. Tada, H., P.C. Paris, and G.R. Irwin, *The stress analysis of cracks handbook*. 3rd ed2000, New York: ASME Press. xx, 677 p.
8. Ju, J.W. and T.M. Chen, *Micromechanics and effective moduli of elastic composites containing randomly dispersed ellipsoidal inhomogeneities.* Acta Mechanica, 1994. **103**(1-4): p. 103-121.

9. Ju, J.W. and T.M. Chen, *Effective elastic moduli of two-phase composites containing randomly dispersed spherical inhomogeneities.* Acta Mechanica, 1994. **V103**(1): p. 123-144.

10. Qu, J. and M. Cherkaoui, *Fundamentals of micromechanics of solids*2006, Hoboken, N.J.: Wiley. xiii, 386 p.

11. Weibull, W., *A Statistical Distribution Function of Wide Applicability.* Journal of Applied Mechanics-Transactions of the Asme, 1951. **18**(3): p. 293-297.

12. Yeni, Y.N. and D.P. Fyhrie, *A rate-dependent microcrack-bridging model that can explain the strain rate dependency of cortical bone apparent yield strength.* J. Biomech., 2003. **36**: p. 1343-1353.

13. Sasaki, N. and S. Odajima, *Stress-strain curve and young's modulus of a collagen molecule as determined by the X-ray diffraction technique.* Journal of Biomechanics, 1996. **29**(5): p. 655-658.

14. Gilmore, R.S. and J.L. Katz, *Elastic properties of apatites.* Journal of Materials Science, 1982. **V17**(4): p. 1131-1141.

15. Akkus, O., *Elastic deformation of mineralized collagen fibrils: An equivalent inclusion based composite model.* Journal of Biomechanical Engineering-Transactions of the Asme, 2005. **127**(3): p. 383-390.

16. Hellmich, C., J.F. Barthelemy, and L. Dormieux, *Mineral-collagen interactions in elasticity of bone ultrastructure - a continuum micromechanics approach.* European Journal of Mechanics a-Solids, 2004. **23**(5): p. 783-810.

17. Fritsch, A. and C. Hellmich, *`Universal' microstructural patterns in cortical and trabecular, extracellular and extravascular bone materials: Micromechanics-based prediction of anisotropic elasticity.* Journal of Theoretical Biology, 2007. **244**(4): p. 597-620.

18. Lees, S., et al., *The loci of mineral in turkey leg tendon as seen by atomic force microscope and electron microscopy.* Calcified Tissue International, 1994. **55**(3): p. 180-189.

19. Sasaki, N., et al., *Atomic force microscopic studies on the structure of bovine femoral cortical bone at the collagen fibril-mineral level.* Journal of Materials Science-Materials in Medicine, 2002. **13**(3): p. 333-337.

20. Weiner, S. and H.D. Wagner, *The material bone: Structure mechanical function relations.* Annual Review of Materials Science, 1998. **28**: p. 271-298.

21. Barber, A.H. and F. Hang, *Nano-mechanical properties of individual mineralized collagen fibrils from bone tissue.* Journal of the Royal Society Interface, 2011. **8**(57): p. 500-505.